Neuro-Oncology 12(6):559–569, 2010.
doi:10.1093/neuonc/nop058
Advance Access publication February 15, 2010

Cellular and in vivo activity of a novel PI3K inhibitor, PX-866, against human glioblastoma

Dimpy Koul, Ruijun Shen, Yong-Wan Kim, Yasuko Kondo, Yiling Lu, Jim Bankson, Sabrina M. Ronen, D. Lynn Kirkpatrick, Garth Powis, and W. K. Alfred Yung

Brain Tumor Center, Department of Neuro-Oncology (D.K., R.S., Y.-W.K., Y.K., W.K.A.Y.), Department of Systems Biology (Y.L.), Department of Imaging Physics (J.B.), Department of Experimental Diagnostic Imaging (S.M.R), and Department of Experimental Therapeutics (G.P.), The University of Texas M. D. Anderson Cancer Center, Houston, Texas; Oncothyreon Inc., Seattle, Washington (D.L.K.)

The phosphatidylinositol-3-kinase (PI3K)/Akt oncogenic pathway is critical in glioblastomas. Loss of PTEN, a negative regulator of the PI3K pathway or activated PI3K/Akt pathway that drive increased proliferation, survival, neovascularization, glycolysis, and invasion is found in 70%–80% of malignant gliomas. Thus, PI3K is an attractive therapeutic target for malignant glioma. We report that a new irreversible PI3K inhibitor, PX-866, shows potent inhibitory effects on the PI3K/Akt signaling pathway in glioblastoma. PX-866 did not induce any apoptosis in glioma cells; however, an increase in autophagy was observed. PX-866 inhibited the invasive and angiogenic capabilities of cultured glioblastoma cells. In vivo, PX-866 inhibited subcutaneous tumor growth and increased the median survival time of animals with intracranial tumors. We also assessed the potential of proton magnetic resonance spectroscopy (MRS) as a noninvasive method to monitor response to PX-866. Our findings show that PX-866 treatment causes a drop in the MRS-detectable choline-to-NAA, ratio and identify this partial normalization of the tumor metabolic profile as a biomarker of molecular drug action. Our studies affirm that the PI3K pathway is a highly specific molecular target for therapies for glioblastoma and other cancers with aberrant PI3K/PTEN expression.

Received March 10, 2009; accepted September 28, 2009.

Present address: *Department of Radiology and Biomedical Imaging, University of California–San Francisco, San Francisco, California (S.M.R.); Ensyce Biosciences Inc., Houston, Texas (D.L.K.)*

Corresponding Author: W.K. Alfred Yung, MD, Department of Neuro-Oncology, Unit 100, The University of Texas M. D. Anderson Cancer Center, 1515 Holcombe Boulevard, Houston, TX 77030 (wyung@mdanderson.org).

Keywords: autophagy, bioavailability, cell cycle arrest, glioma, in vivo, PI3K inhibition, PX-866, safety.

Phosphatidylinositol-3-kinases (PI3Ks) are important in controlling various aspects of the malignant phenotype, including proliferation, survival and apoptosis, adhesion and mobility, angiogenesis, and cell size. The PI3K pathway is activated by loss of the *PTEN* gene and also by amplification and mutation of the *PIK3CA* gene, which encodes the p110α PI3K isoform. The PI3K pathway is the most frequently activated pathway in sporadic human tumors; estimates suggest that mutation in one or more PI3K pathway components accounts for up to 30% of all human cancers.[1] PI3K is activated by both receptor tyrosine kinases and Ras, and PI3K activation in turn activates several downstream signaling pathways through the generation of the lipid second messenger phosphatidylinositol-3,4,5-trisphosphate. In particular, the Akt family (also known as protein kinase B) of serine/threonine kinases has emerged as a critical downstream target of PI3K in human cancer.

Some of the first direct evidence that PI3K deregulation has a role in human cancer was the discovery that genes encoding the p110α PI3K catalytic subunit and Akt are amplified in ovarian, breast, and pancreatic cancer.[1] Also, mutations in the gene encoding the PI3K regulatory subunit p85 were found in some primary colon and ovarian tumors.[2] Strikingly, a large-scale effort to sequence exons of *PI3K* genes from human tumors revealed clustered regions of point mutations in the p110α catalytic subunit in 20%–30% of the breast, colon, brain, and gastric tumors examined.[3] Investigations of the most frequent p110α tumor mutations have shown that the mutations enhance PI3K activity and drive cell transformation.[4] Sequencing of

exons from genes encoding components of the PI3K pathway have revealed point mutations in Akt2 and 3-phosphoinositide-dependent protein kinase 1, amplifications of Akt2 and insulin receptor substrate 2, and mutations in PIK3CA (p110α) and *PTEN* (a negative regulator of the PI3K pathway).[5] Activating mutations in *PIK3CA* have been observed in anaplastic oligodendrogliomas, anaplastic astrocytomas, glioblastoma multiforme tumors, and medulloblastomas, as well as other common malignancies.[6,7] *PIK3CA* and *PTEN* mutations have been observed to occur simultaneously in endometrial tumors and glioblastoma multiforme, indicating a potential additive effect of these two mutations on pathway activation.[8–10] Furthermore, 100% (5 of 5) glioblastoma multiforme tumors with *PIK3CA* mutations also had 10q loss of heterozygosity,[9] suggesting that *PTEN* may be haploinsufficient when other mutations serve to upregulate signaling through the PI3K pathway.[11]

Since abnormalities in PI3K pathway signaling can render cells sensitive to the effects of specific molecular therapeutics, PI3K inhibitors are likely to follow receptor tyrosine kinase inhibitors as the next major class of targeted drugs.[3] It remains to be determined which PI3Ks should be targeted for particular diseases and to what extent the inhibition of these kinases will impair normal physiology.

In the study reported here, we evaluated the action and therapeutic potential of a potent PI3K inhibitor, PX-866, in the treatment of human glioblastoma. PX-866 is a biologically stable synthetic viridin related to wortmannin[12] and was chosen from a library of over 100 wortmannin analogs.[13,14] Wortmannin inhibits all PI3K isoforms and has shown antitumor activity against tumor xenografts in animals,[13] but it is a biologically unstable molecule and is therefore not a good drug candidate. Like wortmannin, PX-866 inhibits PI3K by binding covalently to Lys-802 of the catalytic site of p110α (more potently than wortmannin)[15] and Lys-883 of p110γ;[16] PX-866 also inhibits p110δ. However, unlike wortmannin, PX-866 is a weak inhibitor of PI3K p110β and so shows much reduced dose-limiting on-target toxicity common to PI3K inhibitors.[17] In the present study, we have shown that PX-866 inhibits the activity of target genes in the PI3K/Akt/mTOR cascade and significantly prolongs the median survival of animals with intracranial xenograft tumors without causing any obvious toxic effects. These data suggest that PX-866 inhibition of the PI3K/Akt pathway is a safe and effective therapy for cancers with aberrant PTEN/PI3K expression. In addition, we have shown that magnetic resonance spectroscopy (MRS) may be helpful in monitoring the early molecular response as a noninvasive biomarker of response to PX-866 treatment.

Materials and Methods

Cell Lines

U251, U87, LN229, and LN18 glioblastoma cells were maintained as monolayer cultures in Dulbecco's modified Eagle's medium/F12 supplemented with 10% fetal bovine serum and penicillin–streptomycin (all from Life Technologies, Inc., Grand Island, New York). U251 and U87 are PTEN negative, whereas LN18 and LN229 are PTEN wild-type glioma cells.

Antibodies and Western Blotting

Subconfluent monolayers of cells were treated with PX-866 at various doses in serum-free medium. Four hours later, cells were harvested either stimulated with epidermal growth factor (EGF; 50 ng/mL) for 10 minutes or left untreated. Cells were harvested in lysis solution as described previously[18] and subjected to Western blotting. Membranes were probed with the following primary antibodies: phospho-specific Akt (Ser-473 and Thr-308), total Akt, phospho-MAPK (Thr-202 and Tyr-204), total MAPK, phospho-S6K1, total S6K1, phospho-S6, total S6, and phospho-Rb-S807/S811 (Cell Signaling, Boston, Massachusetts); cyclin D1, cyclin E, and Rb (Santa Cruz Biotechnology, Santa Cruz, California); and p27Kip1 (Transduction Laboratories, San Jose, California). Anti-β-actin antibody was purchased from Sigma (St Louis, Missouri).

Cell Proliferation Assay and Cell Cycle and Autophagy Analyses

The antiproliferative effect of PX-866 on cells growing in culture was determined using the sulforhodamine B assay as described previously.[19] For cell-cycle analysis, 3×10^5 glioblastoma cells were plated per well on 60-mm plates (Costar, Cambridge, Massachusetts) and maintained in 10% fetal bovine serum-containing medium overnight. The next day, the cells were treated with 0.4 and 0.8 μM PX-866. Seventy-two hours later, cells were pelleted, resuspended in 1 mL of 50 μg/mL propidium iodide in phosphate-buffered saline (PBS) containing 20 μg/mL RNase for a further 30 minutes, and then analyzed for DNA content using a FACSCalibur Flow Cytometer and CellQuest software (BD Biosciences, San Jose, California) for any cell-cycle change. For autophagy analysis, cells were plated in a 6-well plate and treated with 0.8 μM of PX-866 for 72 hours, after which the medium was removed and the cells were incubated in 1 μg/mL acridine orange solution at 37°C for 15 minutes. Cells were then trypsinized, resuspended in PBS, and analyzed for autophagy using the flow cytometer and software named above.

In addition, cells were transiently transfected glioma cells with the green fluorescent protein-tagged microtubule-associated protein light chain 3 (GFP-LC3) expression vector using the FuGENE 6 transfection reagent (Roche Applied Science, San Francisco, CA) for 24 hours, treated them with or without 0.8 μM of PX-866, fixed the cells with 4% paraformaldehyde, and determined the proportion of cells expressing GFP-LC3 dots (10 dots/cell) under a fluorescence microscope, as described previously.[20]

Cell Invasion Assay and Enzyme-Linked Immunosorbent Assay for Vascular Endothelial Growth Factor

Cells were treated with 0.8 μM PX-866 for 24 hours, and invasion was assessed by counting the number of cells invading through Matrigel-coated transwell inserts as described previously.[21] To measure vascular endothelial growth factor (VEGF), we treated subconfluent cells with 0.4 and 0.8 μM PX-866. After a 24 hour incubation, the cell cultures were rinsed twice with serum-free medium, and 24 hours later, conditioned medium was collected and clarified by centrifugation at 4000 × *g* for 5 minutes at 4°C; the supernatants were frozen and stored at −80°C until use. The levels of VEGF were measured in conditioned medium samples with the Quantikine ELISA kit (R&D Systems, Minneapolis, Minnesota) according to the manufacturer's instructions.

Animal Studies and MRS

All animal studies were conducted in the veterinary facilities of The University of Texas M. D. Anderson Cancer Center (Houston, Texas) in accordance with institutional, state, and federal laws and ethical guidelines for experimental animal care. We examined the antitumor efficacy of PX-866 in intracranial and subcutaneous xenografts derived from U87 cells. Nude (*nu/nu*) 6–8-week-old mice were obtained from the breeding facility at M. D. Anderson Cancer Center.

To create the intracranial disease model, we engrafted U87 human glioblastoma cells (5×10^5) into the caudate nucleus of athymic mice using a previously described guide-screw system.[22] Starting on day 4 after the tumor cells were implanted, mice were treated by gavage with 2 mg/kg PX-866 in PBS or PBS alone (control) on a 5-days-on, 2-days-off schedule for 4 weeks. Each group had 10 animals; 2 animals from each group were euthanized at 2 weeks and at 4 weeks for biology studies. At necropsy, all organs were analyzed grossly and microscopically to assess toxicity.

For the subcutaneous model, 3×10^6 cells were implanted in the flanks of athymic nude mice. Tumor diameters were measured with vernier calipers twice a week. The mice were treated, starting on day 4 after tumor implantation, with PX-866 (2.0 mg/kg/day by oral gavage; 5 days a week for 4 weeks).

For magnetic resonance imaging (MRI) and proton MRS studies, tumor cells were implanted using nonferromagnetic screw guides 1 mm anterior and 1.2 mm lateral to the bregma; the animals then followed a treatment schedule similar to that described in the preceding paragraph. All spectroscopic and imaging measurements were conducted using a 7.0-T Biospec USR imaging system (Bruker Biospin, Billerica, Massachusetts). A linear volume resonator with an inner diameter of 72 mm was used for signal excitation in mini-imaging gradients (116-mm inner diameter). An electronically tuned, actively decoupled custom radiofrequency coil (13-mm inner diameter) was used for signal detection. A 3-plane rapid acquisition with relaxation enhancement (RARE) imaging sequence was used to confirm positioning, and axial and sagittal multislice T_2-weighted images (TE/TR = 60 ms/3000 ms, RARE factor = 8, 4 averages, 156 μm × 156 μm × 1 mm resolution) were collected for tumor visualization. Following automatic and manual shim adjustment, point-resolved spectroscopic measurements (TE/TR = 20 ms/2500 ms, bandwidth = 4 kHz, 200 averages, 2048 points) with and without water suppression were acquired over cuboid volumes (voxels) ranging from 1.5 to 80 mm^3 (depending on the tumor size) localized inside the tumor only. To compare the spectra of the tumors with those of normal brain tissues, we also placed a voxel in the unaffected region in the contralateral hemisphere. Tumor dimensions were determined from the MR image, and tumor volume was calculated using the formula $(\pi/6) \times \text{length} \times \text{width} \times \text{depth}$. Spectra were analyzed using the MestReC software (Mestrelab Research, Santiago de Compostela, Spain) by determining individual metabolite levels and calculating metabolite ratios. Means and *SD*s were calculated.

Reverse-Phase Protein Lysate Microarray

Reverse-phase protein lysate microarray (RPPA) was performed in our laboratory as described previously.[23] Briefly, lysis buffer was used to lyse mouse xenografts by homogenization. Tumor lysates were normalized to 1 μg/μL concentration using a bicinchoninic acid assay and boiled with 1% sodium dodecyl sulfate, and the supernatants were manually diluted in 6 or 8 2-fold serial dilutions with lysis buffer. A GeneTAC arrayer (Genomic Solutions, Inc., Ann Arbor, Michigan) created 1152 spot arrays on nitrocellulose-coated FAST slides (Schleicher & Schuell BioScience, Inc., Keene, New Hampshire) from the serial dilutions. Each slide was probed with a validated primary antibody, and the signal was amplified using a Dako Cytomation-catalyzed system (Carpinteria, California). The slides were scanned, analyzed, and quantitated using Microvigene software (VigeneTech, Inc., Carlisle, Massachusetts).

Statistical Analyses

For the in vitro experiments, statistical analyses were done using a 2-tailed Student's *t*-test. Data are given as the mean ± *SD*. The in vivo therapeutic efficacy of PX-866 was assessed by plotting the Kaplan–Meier survival curves of animals, and group data were compared with using the log-rank test.

Results

PX-866 Blocks Activation of PI3K-Mediated Signaling in Glioblastoma Cells

In this study, we evaluated the time- and dose-dependent effects of PX-866 on PI3K signaling in glioblastoma cells in vitro. Since EGFR becomes activated on binding to

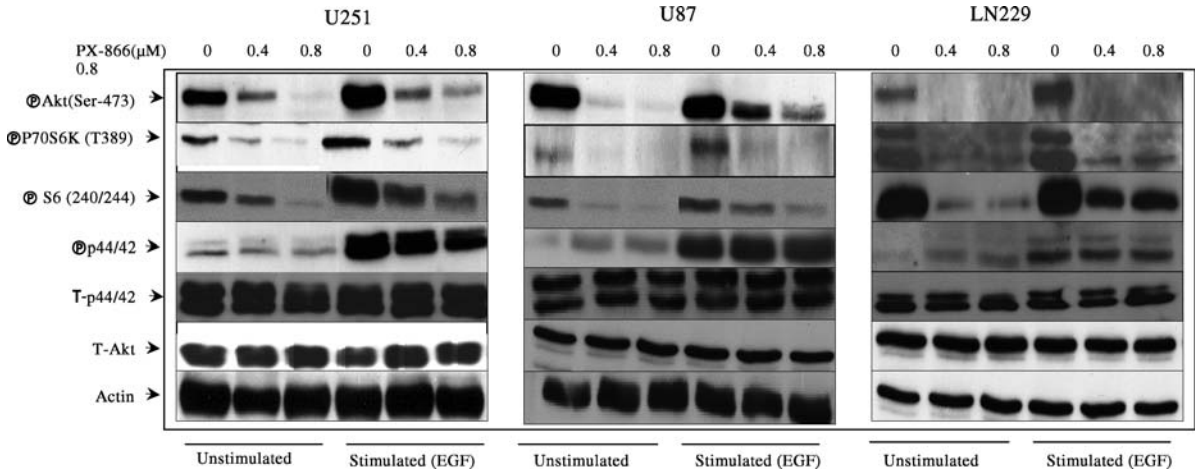

Fig. 1. Effect of PX-866 on signal transduction pathways. Western blot analysis of U251, U87, and LN229 glioblastoma cells was performed as follows: cells were serum-starved for 24 hours and treated with different concentrations of PX-866 as described in the Materials and Methods section. Cells were either left starved or stimulated with EGF (50 ng/mL) for 10 minutes before harvest. The results show that PX-866 inhibited phosphorylation of Akt at Ser-473 without modifying levels of total Akt protein (T-Akt). PI3K downstream targets, including p70S6K and pS6, were also inhibited. PX-866 did not affect phospho- or total MAPK expression. Equal loading was confirmed by immunoblotting with antiactin antibody. Data shown are a representative immunoblot of 3 independent experiments.

EGF and recruits PI3K to the cell membrane. PI3K converts phosphatidylinositol-4,5-bisphosphate (PIP_2) to the second-messenger molecule PIP_3. This second messenger then activates downstream effector molecules, such as Akt and the mammalian target of rapamycin (mTOR), which help induce cellular proliferation and block apoptosis. We found that PX-866 blocked both the basal and EGF-induced phosphorylation of Akt at concentrations as low as 400 nM (Fig. 1). PX-866 also reduced the activation of intracellular Akt downstream targets, including p70S6K and pS6. However, PX-866 did not inhibit basal and EGF-induced MAPK activation, suggesting that PX-866 selectively blocks the PI3K/Akt pathway.

PX-866-Mediated Glioblastoma Cell Growth Inhibition Is Associated with G1 Cell-Cycle Arrest

To determine the signaling pathways implicated in the proliferation of glioblastoma cells, we studied the proliferation of human glioblastoma cell lines U87, U251, LN229, and LN18 in the presence of PX-866. PX-866 dramatically inhibited the proliferation of all the cell lines tested (Supplementary material, Fig. S1). The cell lines we used included cells expressing mutated or wild-type p53 or PTEN proteins. Specifically, p53 is mutated in U251 (at codon 273), LN229 (codon 98), and LN18 (codon 238) and is wild type in U87. PTEN is mutated in U87 (deletion in exon 3) and U251 (frame shift) and is wild type in LN229 and LN18. A differential pattern of sensitivity was observed in this study with PTEN status of glioma cell lines with lower IC50 values for PTEN-negative cell lines. Thus, the IC50 observed for U87 and U251, PTEN-negative cell lines, was 3-fold lower than the one obtained for LN229 and LN-18, wild-type PTEN cell lines. This interesting finding needs to be further confirmed against a broader panel of glioma cells and in in vivo settings.

Treatment with PX-866 induced a marked increase in the number of U251 and U87 cells in the G1 phase after 48 hours (Fig. 2A), as measured by propidium iodide staining and flow cytometry. Therefore, we explored the effect of PX-866 on cell cycle checkpoint signaling by determining the levels or activity of cyclin D1, cyclin E, and p27Kip1. In PX-866-treated cells, cyclin D1 expression decreased (Fig. 2B) in comparison to control cells. The effect of the cyclin D1 decrease on the activity of cyclin D/CDK4 complexes was evaluated by measuring the phosphorylation of Rb by cyclinD/CDK4 with a phospho-Rb-specific antibody that recognizes residues phosphorylated only by cyclin D/CDK4 (Fig. 2B). The phosphorylation of Rb was strongly reduced in the PX-866-treated cells, indicating that the decrease in the cyclin D1 level was accompanied by a strong decrease in cyclin D/CDK4 complex levels. No effect on cyclin E was observed (Fig. 2B).

PX-866 Induces Autophagic Cell Death in Glioblastoma Cells

We tested whether PX-866 induced autophagy, which is characterized by the development of acidic vesicular organelles (detected and measured by the vital staining of acridine orange). As shown in Supplementary material, Fig. S2A (available online), PX-866 induced acidic vascular organelles in a dose-dependent manner in U87 cells; the percentage of cells with acidic vascular organelles ranged from 0.8% to 15.7%. We also assessed the presence of a punctate pattern of the GFP-LC3 expression to determine whether PX-866 induces autophagy in malignant glioma cells. U87 cells were transiently transfected with a GFP-LC3 expression

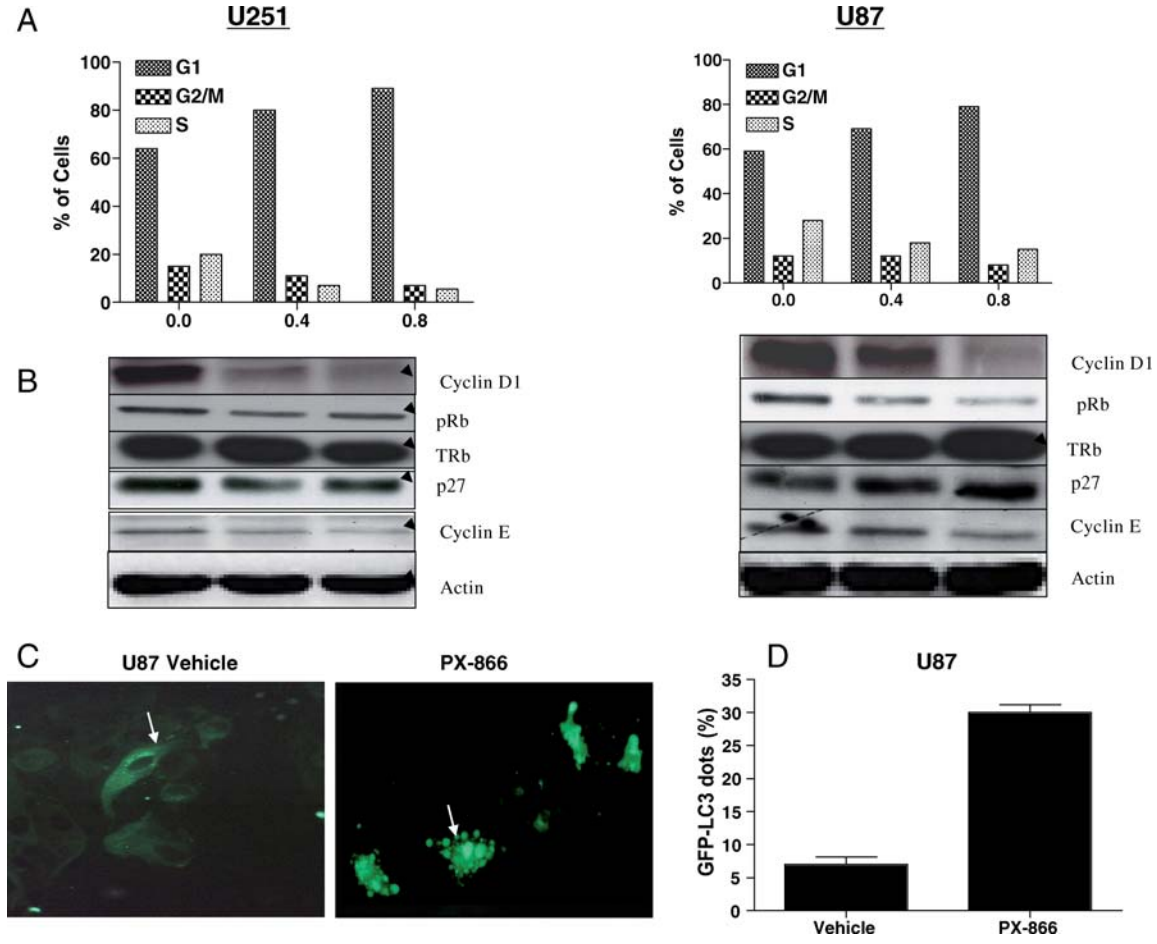

Fig. 2. Effect of PX-866 on cell cycle distribution and autophagic cell death. (A) U251 and U87 cells were treated with PX-866 for 72 hours, stained with propidium iodide, and analyzed by flow cytometry as described in the Materials and Methods section. (B) U251 and U87 cells were incubated for 72 hours with the indicated dose of PX-866. Cells were then lysed, and cell extracts were analyzed by Western blotting for cyclin D1, pRb, p27, and cyclin E. Decreases in cyclin D1 and pRb levels and an increase in the p27Kip1 level in PX-866-treated cells were characteristic of cell cycle arrest in the G1 phase. Data shown are a representative immunoblot of three independent experiments. (C) U87 cells transfected with GFP-LC3 expression vector were treated with vehicle alone or 0.8 μM PX-866 for 48 hours to test for autophagy. Arrows, representative autophagic cells with GFP-LC3 dots. (D) Quantification of autophagic U87 cells treated as described in (C). Results shown are the means ± *SD* of three independent experiments. $P < .01$ compared with vehicle alone.

vector for 24 hours and then treated with vehicle alone or PX-866 (0.8 μM) for an additional 48 hours, as described previously.[20] Under a fluorescence microscope, the vast majority (30%) of the GFP-LC3-transfected cells showed diffuse distribution of GFP-LC3 in the absence of PX-866, whereas treatment with PX-866 often resulted in a punctate pattern of GFP-LC3 fluorescence (Fig. 2C and D). This pattern represents the presence of autophagic vacuoles and indicated that LC3 is recruited to autophagic vacuoles in U87-MG cells treated with PX-866.

We also examined the expression of the LC3 proteins, a hallmark of cells undergoing autophagy. Results from the immunoblotting analysis with anti-LC3 antibody indicate that LC3 is involved in PX-866-induced autophagy and that PX-866 stimulates the conversion of a fraction of LC3-I into LC3-II. PX-866 treatment showed a dramatic change in the ratio of cytosolic LC3-I to membrane-bound LC3-II,[24] a modification that is essential for the induction of autophagy and there was an increase in the ratio of LC3-11/LC3-1 in PX-866-treated tumors in comparison to vehicle-treated tumors. This is shown in Supplementary material, Fig. S2B

PX-866 Inhibits Glioblastoma Cell Invasion

To study whether PI3K plays an important role in cell invasion, we performed a Matrigel invasion assay and counted the number of invasive cells before and after treatment with 0.8 μM of PX-866. We found that glioblastoma cells (LN229 and U251) treated with PX-866 had a cell invasion rate one tenth that of cells treated with medium alone (Fig. 3A). Quantitative analysis showed that 32% of the LN229 cells and 28% of the PX-866-treated U251 cells invaded to the lower side of the membrane, compared with 100% of the parental LN229 and U251 control cells (Fig. 3B). This PX-866-mediated PI3K inhibition of glioblastoma cell

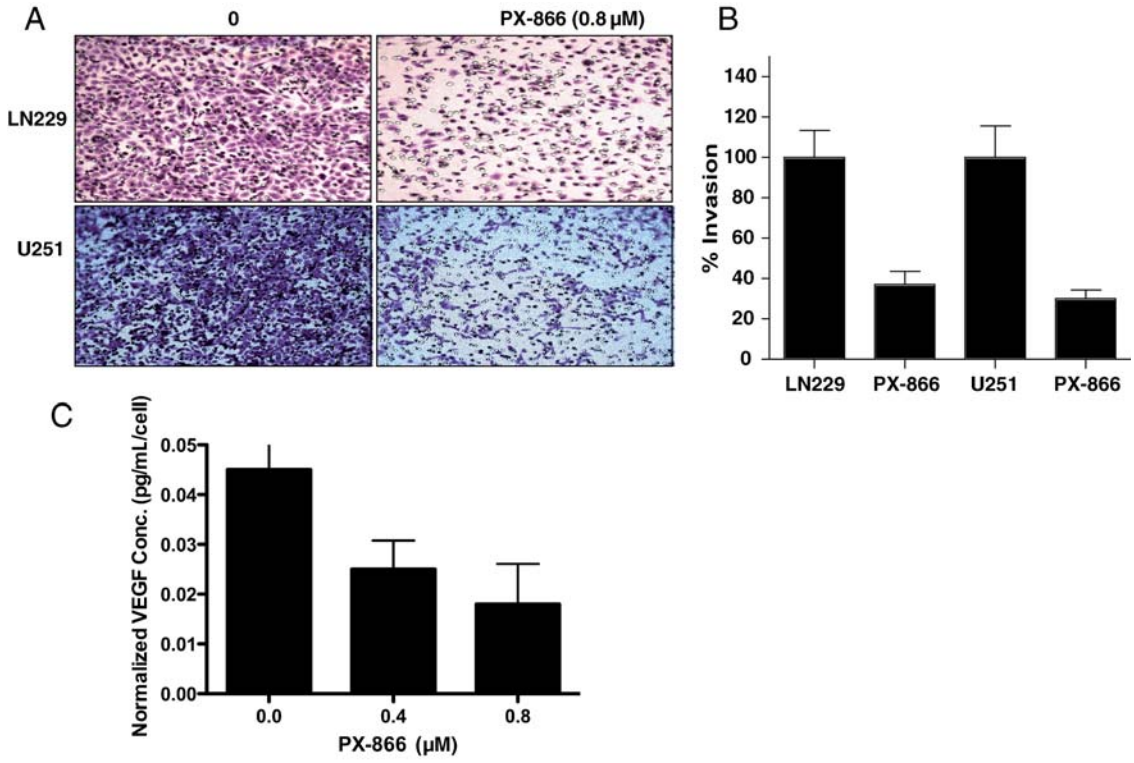

Fig. 3. PX-866 inhibition of transwell invasion and reduction in VEGF secretion. (A) LN229 and U251 cells were treated with PX-866 for 24 hours and replated onto Matrigel-coated inserts. After 24 hours, cells that had migrated to the opposite side were stained with crystal violet. (B) The membranes with invaded cells were dissolved in 2% deoxycholic acid and read colorimetrically at 595 nm for quantification of invasion. (C) PX-866 decreased VEGF secretion by at least 45%–50% in U87 cells. The VEGF level in serum-free medium was measured in triplicate and the experiment repeated at least twice to confirm results. The amount of secreted VEGF was expressed as pg/mL/cell, as described in the Materials and Methods section.

invasion suggests that PI3K is an important therapeutic target.

Inhibition of PI3K by PX-866 Decreases VEGF Secretion in Glioblastoma Cells

VEGF is a principal mediator of angiogenesis, an important element of cancer progression and one of the hallmarks of tumor metastasis.[25] It has been reported that the PI3K/Akt signaling pathway mediates angiogenesis and the expression of VEGF in cells. We found that conditioned medium from PX-866-treated U87 human glioblastoma cells inhibited VEGF secretion in a dose-dependent manner (Fig. 3C) as determined by an enzyme-linked immunosorbent assay. Considering the slower proliferative rate of PX-866 treated cells, we normalized the VEGF level by cell number. Even after normalizing by the cell number, we still observed a 65% decrease in VEGF secretion by PX-866. Because the PI3K/Akt signaling pathway is important in glioblastoma development and PI3K/Akt stimulation results in the stimulation of VEGF, these data confirm that inhibition of PI3K activity can result in substantial inhibition of the expression and therefore the secretion of VEGF.

PX-866 Treatment Is Safe and Effective in an Intracranial Glioblastoma Xenograft Model

For the subcutaneous model, tumor volume was determined at regular intervals according to the formula volume $= l^2w^2/2$, where l is the length and w the width. The mean tumor size $\pm$ *SD* was significantly smaller in the mice treated with PX-866 (320 ± 3.1 mm^3, $n = 10$) than in the control mice (2000 ± 8.1 mm^3, $n = 10$; $P < .002$ by a 2-tailed Student's *t*-test). All the tumors treated with PX-866 showed growth inhibition, and mean tumor volume decreased by 84% (Fig. 4A). The antitumor efficacy of PX-866 was also evaluated in the U87 intracranial tumor model. The median survival time of the control mice (ie, those injected with PBS) was 32 days and the mice treated with PX-866 (Fig. 4B) was significantly longer at 39 days (95% CI = 36–45 days; ($P \leq .001$; log-rank test). Mice treated with PX-866 had no obvious signs of toxic effects with respect to body weight, water intake, and general activity.

After the mice were sacrificed, brains were removed, and tumors were either snap-frozen for protein analysis or fixed in formalin, embedded in paraffin, sectioned, and stained. Microscopic examination of the brains of control mice revealed no infiltrative tumors growing in

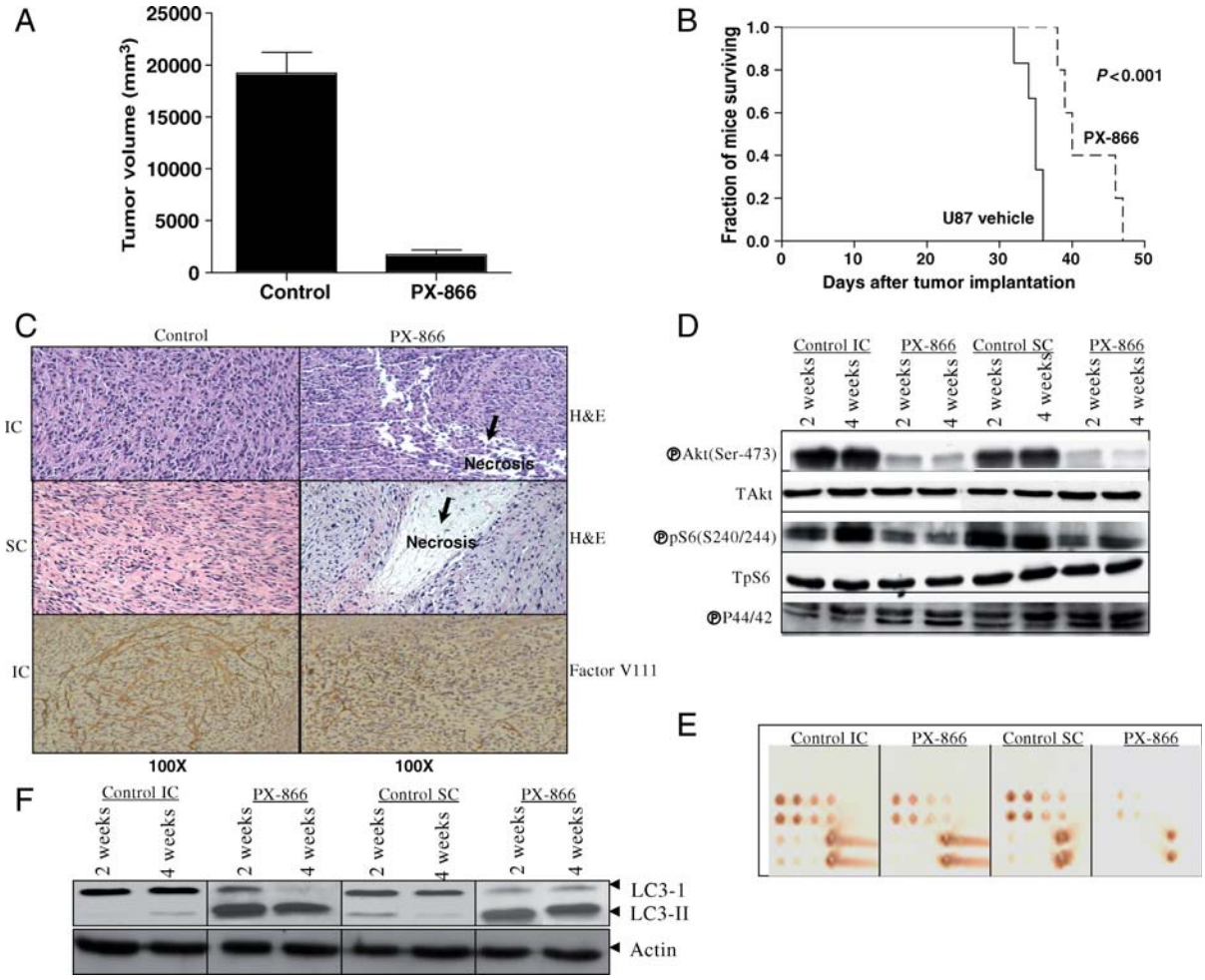

Fig. 4. PX-866 reduction in glioblastoma growth in vivo. (A) U87-tumor-bearing mice were treated with PX-866 (2.0 mg/kg/day by oral gavage; 5 days a week for 4 weeks). Tumor volumes were measured twice a week during the course of the experiment. The mean tumor volume was reduced by 84% in U87 flank xenografts treated with PX-866. (B) Kaplan–Meier survival curve of animals with intracranial U87 tumors. PX-866 increased the median survival time from 32 to 39 days ($P \leq .001$; log-rank test). (C) Examination of the brains of control mice revealed hypercellular areas, whereas examination of the brains of PX-866-treated mice revealed necrotic lesions in both subcutaneous (SC) and intracranial (IC) tumors. The tumor microvessel densities in the tumor tissues were determined by staining with an antifactor VIII antibody [anti-von Willebrand factor (vWF)]. The staining patterns and quantifications shown were representative of those observed in 10 random fields. Note that the PX-866-treated tumor showed decreased microvessel densities in brain tumors. Magnification: ×100. (D) Immunoblotting analyses of both expression and activation of Akt and S6K1 in 2- and 4-week tumors following PX-866 treatment. Immunoblotting analyses demonstrated that PX-866 inhibited the activity of S6K1 in both sets of tumors, as assessed by the level of the corresponding phosphorylated protein. (E) The same lysates were analyzed by RPPA. Five nanograms of cellular protein for the first spot of each sample were spotted for RPPA. Each spot represents a dilution of the sample. The slide was probed for p-Akt (Ser-473), and both IC and SC tumor lysates showed blockade of p-Akt after PX-866 treatment. (F) Immunoblotting analyses to assess LC3-II expression after 2- and 4-week tumor cell extracts following PX-866 treatment. The increase in the ratio of LC3-II/LC3-I is an indication of autophagy in PX-866-treated tumors in comparison to vehicle-treated animals.

a spherical pattern, with a high level of cell proliferation and hypervascularity and an absence of necrosis. In contrast, microscopic examination of the brains of mice treated with PX-866 revealed necrosis and cellular debris (Fig. 4C). Immunohistochemical analysis further showed a significant reduction in factor VIII-positive staining in PX-866-treated tumor sections as compared with control sections, suggesting that PX-866 may be involved in inhibiting tumor angiogenesis in vivo (Fig. 4C).

In addition, as measured by the percentage of cells expressing Ki-67, control tumors displayed hypercellular areas with high mitotic numbers, whereas PX-866-treated cells showed decreased proliferation (Supplementary material, Fig. S3A).

The antitumor effect was also evidenced by decreased levels of phosphorylated Akt and S6 in the tumor tissues, consistent with a blockade of PI3K, as revealed by Western blotting and RPPA of tumor extracts (Fig. 4D and E) or immunohistochemical analyses of tumor

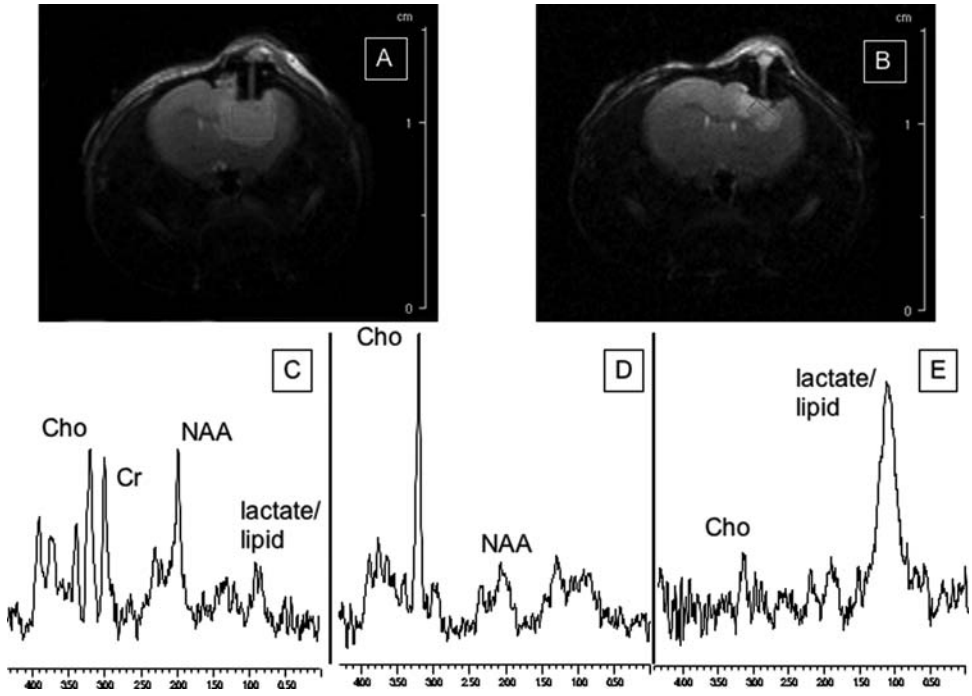

Fig. 5. MRI- and MRS-detectable changes after PX-866 treatment. T2-weighted MR images of control (A) and PX-866-treated (B) intracranial U87 tumors; ^{1}H spectra of (C) contralateral brain in control, untreated animal; (D) untreated tumor in the same animal; and (E) a PX-866-treated tumor.

sections (Supplementary material, Fig. S3B). In addition, the lysates of tumor tissue from animals treated with PX-866 showed a dramatic change in the ratio of cytosolic LC3-I to membrane-bound LC3-II, a modification that is essential for the induction of autophagy, indicating that autophagy is involved in tumor growth retardation in vivo (Fig. 4F).

Characterization of Response of U87 Glioblastoma to PX-866 by MRI and MRS

To determine the effect of PX-866 treatment on glioblastoma tumor size, we studied intracranial U87 tumors by MRI. Tumor volumes decreased significantly after PX-866 treatment; mean tumor volumes $\pm$ *SD* were 20 ± 11 mm^3 in control mice ($n = 10$) and 5 ± 4 mm^3 in PX-866-treated mice ($n = 10$, $P < .002$; Fig. 5A and B).

To assess the potential of MRS-detectable metabolic changes to serve as noninvasive biomarkers of response to PX-866, we also performed localized MRS in control and PX-866-treated mice. The mean choline-to-NAA ratio (Cho/NAA) $\pm$ *SD* of spectra from normal contralateral brain tissue was 0.8 ± 0.1 and PX-886 treatment did not affect the spectra recorded from normal brain tissues. In contrast, spectra from tumors indicated that mean Cho/NAA $\pm$ *SD* was 30% lower in PX-866-treated tumors (1.2 ± 0.5, $n = 10$) than in untreated tumors (1.7 ± 0.4, $n = 10$; $P < .002$). Interestingly, relatively smaller tumors (3.2 ± 0.3 mm^3; $n = 3$) also exhibited a significant elevation in the composite lipid and lactate (lac-lip) peak typically indicative of necrosis (Cho/lac-lip increased from 2 ± 1 to 0.2 ± 0.2; $P < .001$), and in those tumors, Cho/NAA was comparable with normal contra-lateral brain (0.7 ± 0.9; $P = .2$). Thus, PX-866 treatment resulted in smaller tumors with Cho/NAA values closer to those observed in normal brain. Thus, PX-866 treatment resulted in MRS-detectable metabolic changes indicative of partial normalization of the metabolic profile. In addition, we successfully used MRS to noninvasively monitor the molecular effects of PX-866 on glioblastomas in vivo, indicating that MRS could be valuable in monitoring early molecular response to PX-866 in patients.

Discussion

We investigated the role of the PI3K inhibitor PX-866 in a set of well-characterized glioblastoma cell lines and found that PX-866 treatment for 72 hours resulted in dose-dependent growth inhibition. Consistent with its role as a PI3K antagonist, PX-866 inhibited the ability of EGF to induce Akt phosphorylation and also inhibited other PI3K-mediated downstream targets. We suggest here a dual mechanism of PX-866-induced inhibition of PI3K signaling involving (i) downregulation of cell cycle-regulating protein cyclin D1, the synthesis of which is regulated by p70S6K and 4E-BP-1 and involves cell cycle arrest in G1 phase, and (ii) induction of autophagy. This dual mechanism of action of PX-866 may contribute to the efficacy of PX-866 observed in our studies. The antiproliferative activity of PX-866 occurs partly through inhibition of cell-cycle progression in

glioma cells. Regardless of their PTEN status, glioma cells treated with PX-866 showed G_1 cell-cycle arrest with no apparent induction of apoptosis. Thus, apoptosis could not have accounted for the potent effect of PX-866 on glioma cell growth. Recently, several lines of evidence have demonstrated that small-molecular mass inhibitors such as imatinib,[26] curcumin,[20] and temozolomide[27] induce a type II programmed cell death, autophagy, which suggests that autophagy may be a response of tumor cells to the blockage of signals for survival. Therefore, cell-cycle arrest in G1 may directly contribute to autophagy as PX-866 increased LC3 cleavage, and this may represent a highly conserved mitotic or postmitotic checkpoint control of autophagy.[28] It has recently been reported that cooperativity between blockade of PI3K and mTOR signaling impacts autophagy in glioma cells.[29] A similar observation of G_1 cell-cycle arrest has been reported for other PI3K inhibitors.[30]

The PI3K/Akt signaling pathway mediates invasion, angiogenesis, and the expression of VEGF in cells.[31–33] This stimulation of VEGF in cancer cells can be mediated by autocrine or chronic stimulation by growth factors such as insulin-like growth factor-1, constitutive activation of PI3K, or constitutive activation of Akt due to inactivation of the tumor suppressor PTEN.[32,33] Here, we report that inhibition of PI3K by a potent PI3K inhibitor resulted in statistically significant suppression of VEGF secretion. A similar antiangiogenic activity was previously observed for another PI3K inhibitor, SF1326.[34] Importantly, PX-866 also inhibited the invasive potential of both U87 and LN229 cells. Thus, we conclude that PX-866 is directly involved in the inhibition of invasion and angiogenic potential of glioblastoma cells. In addition, in the present study, it was clear that PI3K triggers the invasion and angiogenesis of glioblastoma cells and that the pharmacologic inhibition of this pathway significantly abolishes invasiveness and angiogenesis. Recent studies have shown that the PI3K pathway is an attractive therapeutic target because of its integral role in the regulation of tumor proliferation, invasiveness, and survival.[35] Multiple studies with small interfering RNAs and pharmacologic inhibitors have shown the importance of PI3K blockade, and several agents that target this pathway are already undergoing clinical testing; some have already shown promise in clinical trials.[36,37] For example, LY294002 has been tested in an ectopic skin and orthotopic brain tumor model and has been shown to inhibit glioma tumor growth.[38] LY294002 has also shown efficacy against ovarian carcinoma.[39]

Consistent with these results, we also found therapeutic activity of PX-866 in human tumor xenograft models, where immunohistochemical and RPPA analyses showed that p-Akt and pS6 inhibition were linked to an 84% growth inhibition in a subcutaneous tumor model and an increase in the median survival of mice with intracranial U87 tumors from 32 to 39 days. Also, MRI findings indicated that tumor growth was inhibited approximately 75% after PX-866 treatment. This was similar to the growth inhibition observed in the subcutaneous tumors. Although the increase in survival was only 7 days (30%) more in PX-866-treated animals, this increase in 30% is statistically significant ($P < .001$) in a nude mouse model. Although we have shown adequate targeting of PX-866 to the tumor by showing treatment with PX-866 effectively decreased p-Akt and pS6 in the treated animals using Western blots and the novel RPPA technique, the effectiveness of the treatment does not seem to be so robust due to the activation of a collateral pathway for tumor survival. We believe that tumor heterogeneity and complex compensatory or collateral pathways negate the therapeutic efficacy of suppressing a single node. The logical next step is to identify the compensatory pathways responsible for maintaining cell survival when PI3K is inactivated and suggests that additional refinement of this overall approach is necessary.

As expected, ^{1}H spectroscopy showed a significant difference in the Cho/NAA ratio between tumors and normal contralateral brain tissue, consistent with previous findings, such as those reported by Workman et al.[40] More importantly, PX-866 treatment led to significant alterations in the spectra of treated tumors compared with those of untreated tumors. Specifically, spectra from treated tumors had significantly lower Cho/NAA. This observation is consistent with our previous finding that a drop in phosphocholine, the main component of the choline peak, is associated with PI3K inhibition in cells treated with wortmannin, an analog of PX-866.[41] In addition, our observation that relatively small tumors were characterized by an increase in the lactate–lipid peak typically associated with necrosis in brain tumors[42] is consistent with our histological findings indicating that PX-866 can lead to necrosis. Thus, the drop in Cho/NAA in PX-866 tumors is likely indicative of PI3K inhibition, tumor cell death, and the presence of a larger proportion of cells with normal Cho/NAA. This more normal appearing metabolic signature could predict better long-term response.

In summary, our results affirm that PX-866 is an effective specific inhibitor of PI3K; that the PI3K/Akt pathway is a highly specific molecular target for the development of molecular therapeutics for glioblastoma and other cancers with aberrant PTEN/PI3K expression; and that PX-866 treatment results in MRS-detectable metabolic changes that indicate a partial normalization of the metabolic profile of treated tumors. This illustrates the potential of MRS to noninvasively monitor the molecular effects of PX-866 in glioblastomas in vivo. Further studies monitoring the longitudinal effect of PX-866 treatment need to be performed to confirm the value of MRS in monitoring early molecular response to this PI3K inhibitor in patients.

Supplementary Material

Supplementary material is available at *Neuro-Oncology Journal* online

Acknowledgments

We thank Verlene Henry and Jennifer Edge for performing the animal studies. We thank Stephanie Deming and Kathryn Carnes (Department of Scientific Publications, The University of Texas M. D. Anderson Cancer Center) for editing the manuscript.

Conflict of interest statement. None declared.

Funding

This study was supported by grants from the NIH (CA123304, CA56041, and CA127001-02A1 to W.K.A.Y.; CA052995, CA061015, CA0179094, and CA127001 to G.P.); Accelerate Brain Cancer Cure (to W.K.A.Y. and D.K.); and The University of Texas M. D. Anderson Cancer Center Targeted Therapy Grant (to D.K.).

References

1. Luo J, Manning BD, Cantley WC. Targeting the PI3K-Akt pathway in human cancer: rationale and promise. *Cancer Cell*. 2003;4:257–262.
2. Bader AG, Kang S, Zhao L, Vogt PK. Oncogenic PI 3K deregulates transcription and translation. *Nat Rev Cancer*. 2005;5:921–929.
3. Samuels Y, Diaz LA, Jr, Schmidt-Kittler O, et al. Mutant PIK3CA promotes cell growth and invasion of human cancer cells. *Cancer Cell*. 2004;7:561–573.
4. Samuels Y, Wang Z, Bardelli A, et al. High frequency of mutations of the PIK3CA gene in human cancers. *Science*. 2004;304:554.
5. Parsons DW, Wang TL, Samuels Y, et al. Colorectal cancer: mutations in a signalling pathway. *Nature*. 2005;436:792.
6. Broderick DK, Di C, Parrett TJ, et al. Mutations of PIK3CA in anaplastic oligodendrogliomas, high-grade astrocytomas, and medulloblastomas. *Cancer Res*. 2004;64:5048–5050.
7. Knobbe CB, Reifenberger G. Genetic alterations and aberrant expression of genes related to the phosphatidyl-inositol-3′-kinase/protein kinase B (Akt) signal transduction pathway in glioblastomas. *Brain Pathol*. 2003;13:507–518.
8. Oda K, Stokoe D, Taketani Y, McCormick F. High frequency of coexistent mutations of PIK3CA and PTEN genes in endometrial carcinoma. *Cancer Res*. 2005;65:10669–10673.
9. Hartmann C, Bartels G, Gehlhaar C, Holtkamp N, von Deimling A. PIK3CA mutations in glioblastoma multiforme. *Acta Neuropathol*. 2005;109:639–642.
10. Hayes MP, Wang H, Espinal-Witter R, et al. PIK3CA and PTEN mutations in uterine endometrioid carcinoma and complex atypical hyperplasia. *Clin Cancer Res*. 2006;12:5932–5935.
11. Nelson SJ. Multivoxel magnetic resonance spectroscopy of brain tumors. *Mol Cancer Ther*. 2003;2:497–507.
12. Ihle N, Williams TR, Chow S, et al. Molecular pharmacology and antitumor activity of PX-866, a novel inhibitor of phosphoinositide-3-kinase signaling. *Mol Cancer Ther*. 2004;3:763–772.
13. Schultz RM, Merriman RL, Andis SL, et al. In vitro and in vivo antitumor activity of the phosphatidylinositol-3-kinase inhibitor, wortmannin. *Anticancer Res*. 1995;15:1135–1139.
14. Wipf P, Minion DJ, Halter RJ, et al. Synthesis and biological evaluation of synthetic viridins derived from C(20)-heteroalkylation of the steroidal PI-3-kinase inhibitor wortmannin. *Org Biomol Chem*. 2004;2:1911–1920.
15. Wymann MP, Bulgarelli-Leva G, Zvelebil MJ, et al. Wortmannin inactivates phosphoinositide 3-kinase by covalent modification of Lys-802, a residue involved in the phosphate transfer reaction. *Mol Cell Biol*. 1996;16:1722–1733.
16. Walker EH, Pacold ME, Perisic E, et al. Structural determinants of phosphoinositide 3-kinase inhibition by wortmannin, LY294002, quercetin, myricetin, and staurosporine. *Mol Cell*. 2000;6:909–919.
17. Ihle NT, Paine-Murrieta G, Berggren MI, et al. The phosphatidylinositol-3-kinase inhibitor PX-866 overcomes resistance to the epidermal growth factor receptor inhibitor gefitinib in A-549 human non-small cell lung cancer xenografts. *Mol Cancer Ther*. 2005;4:1349–1357.
18. Koul D, Jasser SA, Lu Y, et al. Motif analysis of the tumor suppressor gene MMAC/PTEN identifies tyrosines critical for tumor suppression and lipid phosphatase activity. *Oncogene*. 2002;21:2357–2364.
19. Rubinstein LV, Shoemaker RH, Paull KD, et al. Comparison of in vitro anticancer-drug-screening data generated with a tetrazolium assay versus a protein assay against a diverse panel of human tumor cell lines. *J Natl Cancer Inst*. 1990;8:1113–1118.
20. Shinojima N, et al. Roles of the Akt/mTOR/p70S6K and ERK1/2 signaling pathways in curcumin-induced autophagy. *Autophagy*. 2007;635–637.
21. Koul D, Parthasarathy R, Shen R, et al. Suppression of matrix metalloproteinase-2 gene expression and invasion in human glioma cells by MMAC/PTEN. *Oncogene*. 2001;11:6669–6678.
22. Lal S, Lacroix M, Tofilon P, et al. An implantable guide-screw system for brain tumor studies in small animals. *J Neurosurg*. 2000;92:326–333.
23. Hennessy BT, Lu Y, Poradosu E, et al. Quantified pathway inhibition as a pharmacodynamic marker facilitating optimal targeted therapy dosing: proof of principle with the AKT inhibitor perifosine. *Clin Cancer Res*. 2007;13:7421–7431.
24. Kabeya Y, Mizushima N, Ueno T, et al. LC3, a mammalian homologue of yeast Apg8p, is localized in autophagosome membranes after processing. *EMBO J*. 2003;19:5720–5728.
25. Hanahan D, Weinberg RA. The hallmarks of cancer. *Cell*. 2000;100:57–70.
26. Ertmer A, et al. The anticancer drug imatinib induces cellular autophagy. *Leukemia*. 2007;5:936–942.
27. Kanzawa T, et al. Role of autophagy in temozolomide-induced cytotoxicity for malignant glioma cells. *Cell Death Differ*. 2004;11:448–457.
28. Veneault-Fourrey C, Barooah M, Egan M, Wakley G, Talbot NJ. Autophagic fungal cell death is necessary for infection by the rice blast fungus. *Science*. 2006;312:580–583.
29. Takeuchi H, Kondo Y, Fujiwara K, et al. Synergistic augmentation of rapamycin-induced autophagy in malignant glioma cells by phosphatidylinositol 3-kinase/protein kinase B inhibitors. *Cancer Res*. 2005;65:3336–3346.
30. Fan QW, Knight ZA, Goldenberg DD, et al. A dual PI3 kinase/mTOR inhibitor reveals emergent efficacy in glioma. *Cancer Cell*. 2006;9:341–349.
31. Semenza GL. HIF-1 and tumor progression pathophysiology and therapeutics. *Trends Mol Med*. 2002;8:S62–S67.
32. Brazil DP, Park J, Hemmings BA. PKB binding proteins getting in on the Akt. *Cell*. 2002;111:293–303.

33. Galetic M, Andjelkovic R, Meier D, Brodbeck Park BJ, Hemmings BA. Mechanism of protein kinase B activation by insulin/insulin-like growth factor-1 revealed by specific inhibitors of phosphoinositide 3-kinase–significance of diabetes and cancer. *Pharmacol Ther.* 1999;82:409–425.
34. Garlich JR, De P, Dey N, et al. A vascular targeted pan phosphoinositide 3-kinase inhibitor prodrug, SF1126, with antitumor and antiangiogenic activity. *Cancer Res.* 2008;68:206–215.
35. Sebolt-Leopold JS. MEK inhibitors: a therapeutic approach to targeting the Ras-MAP kinase pathway in tumors. *Curr Pharm Des.* 2004;10:1907–1914.
36. Panka DJ, Atkins MB, Mier JW. Targeting the mitogen-activated protein kinase pathway in the treatment of malignant melanoma. *Clin Cancer Res.* 2006;12:2371–2375.
37. Maira SM, Stauffer F, Brueggen J, et al. Identification and characterization of NVP-BEZ235, a new orally available dual phosphatidylinositol 3-kinase/mammalian target of rapamycin inhibitor with potent in vivo antitumor activity. *Mol Cancer Ther.* 2008;7:1851–1863.
38. Su JD, Mayo LD, Donner DB, Durden DL. PTEN and phosphatidylinositol 3′-kinase inhibitors up-regulate p53 and block tumor-induced angiogenesis: evidence for an effect on the tumor and endothelial compartment. *Cancer Res.* 2003;63:3585–3592.
39. Hu L, Zaloudek C, Mills GB, Gray J, Jaffe RB. In vivo and in vitro ovarian carcinoma growth inhibition by a phosphatidylinositol 3-kinase inhibitor (LY294002). *Clin Cancer Res.* 2000;6:880–886.
40. Workman P, Aboagye EO, Chung YL, et al. Minimally invasive pharmacokinetic and pharmacodynamic technologies in hypothesis-testing clinical trials of innovative therapies. *J Natl Cancer Inst.* 2006;98:580–598.
41. Beloueche-Babari M, Jackson LE, Al-Saffar NM, et al. Identification of magnetic resonance detectable metabolic changes associated with inhibition of phosphoinositide 3-kinase signaling in human breast cancer cells. *Mol Cancer Ther.* 2006;5:187–196.
42. Zoula S, et al. Correlation between the occurrence of 1H-MRS lipid signal, necrosis and lipid droplets during C6 rat glioma development. *NMR Biomed.* 2003;16:199–212.